LAWRENCE
LIVERMORE
NATIONAL
LABORATORY

LLNL-JRNL-403024

Understanding the anomalous dispersion of doubly-ionized carbon plasmas near 47 nm

J. Nilsen, J. I. Castor, C. A. Iglesias, K. T. Cheng, J. Dunn, W. R. Johnson, J. Filevich, M. A. Purvis, J. Grava, J. J. Rocca

April 17, 2008

High Energy Density Physics

Disclaimer

Understanding the anomalous dispersion of doubly-ionized carbon plasmas near 47 nm

Joseph Nilsen, John I. Castor, Carlos A. Iglesias, K. T. Cheng, James Dunn
Lawrence Livermore National Laboratory, Livermore, CA 94551

Walter R. Johnson
University of Notre Dame, Notre Dame, IN 46556

Jorge Filevich, Michael A. Purvis, Jonathan Grava, Jorge J. Rocca
Colorado State University, Fort Collins, CO 80523

Abstract

Over the last several years we have predicted and observed plasmas with an index of refraction greater than one in the soft X-ray regime. These plasmas are usually a few times ionized and have ranged from low-Z carbon plasmas to mid-Z tin plasmas. Our main calculational tool has been the average atom code. We have recently observed C^{2+} plasmas with an index of refraction greater than one at a wavelength of 46.9 nm (26.44 eV). In this paper we compare the average atom method, AVATOMKG, against two more detailed methods, OPAL and CAK, for calculating the index of refraction for the carbon plasmas and discuss the different approximations used. We present experimental measurements of carbon plasmas that display this anomalous dispersion phenomenon. It is shown that the average atom calculation is a good approximation when the strongest lines dominate the dispersion. However, when weaker lines make a significant contribution, the more detailed calculations such as OPAL and CAK are essential. During the next decade X-ray free electron lasers and other X-ray sources will be available to probe a wider variety of plasmas at higher densities and shorter wavelengths so understanding the index of refraction in plasmas will be even more essential. With the advent of tunable X-ray lasers the frequency dependent interferometer measurements of the index of refraction may enable us to determine the absorption coefficients and line-shapes and make detailed comparisons against our atomic physics codes.

Keywords: X-ray laser, Interferometers; Index of refraction; Plasmas; Anomalous dispersion

1. Introduction

For many decades optical interferometers have been used to measure the index of refraction of plasmas [1]. Using the assumption that the index of refraction of the plasma is due only to the free electrons [1-2], an interferometer can measure the transverse electron density of the plasma since, for a plasma that is spatially uniform in the longitudinal direction, the electron density is directly

proportional to the number of fringe shifts in the interferometer. This assumption also means that the index of refraction in the plasma must be less than one. Over the last decade many interferometers [3-8] have been built in the soft X-ray wavelength range of 14 to 72 nm (89 to 17 eV) to measure the electron density of plasmas assuming the free electron approximation. In the future, interferometers will be built using the X-ray free electron lasers, which will extend lasers to even shorter wavelengths [9] so understanding the regimes of validity for the free electron approximation will be even more vital when these diagnostics are used to measure the electron density of plasmas.

Over the last four years interferometer experiments [10-15] of Al, Sn, Ag, and C plasmas have observed fringe lines bend in the opposite direction than was expected, indicating that the index of refraction was greater than one in parts of the plasma. Analysis of these experiments showed that the anomalous dispersion from the resonance lines and absorption edges of the bound electrons have a larger contribution to the index of refraction with the opposite sign as the free electrons [10-14,16-18] and their influence on the index of refraction extends far from the absorption edges and resonance lines. In all these experiments the familiar dispersion [19] from solid-state physics, which is responsible for glass having an index of refraction between 1.5 and 2.0 and gives us visible optics, appears as an important effect in the plasma regime, where it has traditionally been ignored.

In the course of understanding the anomalous dispersion phenomenon in the plasma regime we have developed a new average atom code [20], given the name AVATOMKG, that enables us to calculate the index of refraction for any plasma at any wavelength. This code is a modified version of the INFERNO average atom code [21] that has been used for many years to calculate the absorption coefficients for plasma at a given temperature and density.

In this paper we compare calculations of the index of refraction for carbon plasmas done with the AVATOMKG code against calculations done with the more detailed OPAL and CAK codes. The different approximations used in the three codes are discussed. It is important to understand the limitations of the various methods and the need for good experimental data to improve the predictive capability of the calculations. We also present experimental measurements of C^{2+} plasmas that have observed the index of refraction greater than one at the 46.9 nm (26.44 eV) wavelength of the Ne-like Ar X-ray laser [22] that is used at Colorado State University. This X-ray laser is a capillary discharge, table-top X-ray laser that has been used for more than a decade as a research tool. The ability to calculate and measure this phenomenon of anomalous dispersion is only in its

infancy and much research needs to be done to improve the capability for accurate quantitative predictions and measurements.

2. Analysis of interferometer experiments

The traditional formula for the index of refraction of a plasma is $n = (1 - N_{elec} / N_{crit})^{1/2}$ where N_{elec} is the electron density of the plasma and N_{crit} is the plasma critical density. This assumes that only free electrons contribute to the index of refraction. At wavelength λ, $N_{crit} = \pi / (r_0 \lambda^2)$ where r_0 is the classical electron radius, 2.81794×10^{-13} cm [2]. In typical experiments the electron density is much smaller than the critical density so the formula above can be approximated by $n = 1 - (N_{elec} / 2N_{crit})$. In an interferometer the number of fringe shifts, N_{fs}, is given by the difference in path length of the two interfering beams as they go through the interferometer, relative to the wavelength of the probe beam:

$$N_{fs} = \frac{1}{\lambda}\int_0^L (1 - n)\,dl \qquad (1)$$

When probing a plasma that is uniform over its length L the expression for the number of fringe shifts observed in an interferometer becomes $N_{fs} = (1 - n)\, L / \lambda$. The number of fringe shifts is measured with respect to a set of reference fringes in the absence of any plasma and, using the approximations described above for a uniform plasma, this simplifies to

$$N_{fs} = \frac{N_{elec} \cdot L}{2\lambda \cdot N_{crit}} \qquad (2)$$

When analyzing an experiment one measures how far the fringes have shifted compared with the reference fringes and converts this into electron density using Eq. (2). For the 46.9 nm Ne-like Ar soft x-ray laser, with a critical density of 5.08×10^{23} cm^{-3}, the number of fringe shifts in the interferogram is given by $N_{fs} = (N_{elec}\, L) / (4.8 \times 10^{18}$ cm$^{-2})$. Under these assumptions, the fringes will always bend in one direction when a plasma is probed, but from the anomalous results observed in many interferometer experiments [10-15] over the last four years it is clear that the traditional

technique used to analyze the interferometer experiments is incomplete and that the bound electrons can have a significant contribution to the index of refraction for many partially ionized plasmas.

An approach to understand the contribution of the bound electrons to the index of refraction is to look at the relationship between the absorption coefficient and the index of refraction. The total absorption coefficient $\alpha = N_{ion}\ \sigma = (4\ \pi\ \beta) / \lambda$ where N_{ion} is the ion density of the plasma, λ is the wavelength, σ is the absorption cross-section, β is the imaginary part of the complex index of refraction n* defined by $n^* = 1 - \delta - i\beta$. The real part of the index of refraction $n = 1 - \delta$. The Henke tables [23] available from Lawrence Berkeley Laboratory (LBL) tabulates the dimensionless optical constants f_2 and f_1 for neutral materials. These coefficients are related to δ and β by $\delta = f_1\ N_{ion} / (2\ N_{crit})$ and $\beta = f_2\ \ N_{ion} / (2\ \ N_{crit})$. From the total absorption cross-section σ we determine the optical constant $f_2 = \sigma / (2\ \lambda\ r_0)$. We then derive the optical constant f_1 as a function of photon energy E using the Kramers-Kronig dispersion relation [24]. This involves taking the principal value of the integral

$$f_1(E) = Z_{nuc} + \frac{2}{\pi} P.V. \int_0^\infty \frac{f_2(\varepsilon)\ \varepsilon\ d\varepsilon}{E^2 - \varepsilon^2} \tag{3}$$

where Z_{nuc} is the atomic number of the element. This means we include the total number of bound and free electrons when calculating the dispersion relation. For example, $Z_{nuc} = 6$ for a C plasma and 50 for a Sn plasma. For neutral materials the oscillator strength sum rules insure that f_1 goes to zero at zero energy and Z_{nuc} at infinite energy. For an ionized plasma with average ionization Z* then $f_1 = Z^*$ at E = 0. Z* is the average number of free electrons per ion.

In the absence of any bound electrons f_1 is equivalent to the number of free electrons per ion. Taking the ratio of f_1 to Z* gives the ratio of the electron density measured using the free electron approximation to the actual electron density in the plasma. When this ratio is negative, the index of refraction is greater than one and the fringes in the interferogram bend in the opposite direction than expected.

To illustrate this phenomena, Fig. 1a shows an interferogram of a 0.1-cm long C plasma taken 3 ns after the creation of the plasma by illuminating a 500 μm semi-cyclindrical C target with 0.6 J of energy from a 120-ps duration Ti:Sapphire laser. The solid lines indicate the position of the reference fringes in the absence of any plasma. In the interferogram one observes the highest density plasma in the center of the cylinder with the fringes moving to the right, as expected. However, near

the surface of the target one observes fringes that move to the left of the reference fringes, indicating the index of refraction is great than one in this region. Fig. 1b shows a map of the calculated number of fringe shifts from the interferogram in Fig. 1a. In the region near the center of the cylinder one finds up to 1.5 positive fringe shifts, but surrounding this region, and especially near the target walls, negative fringe shifts are observed of up to -1. Closer to the target surface the absorption of the probe beam prevents measurements of the number of fringe shifts. This is consistent with the central high-density region being sufficient hot and ionized (three or more times ionized) such that the free electron approximation for the index of refraction is valid. However, in the cooler region near the target surface where the C is less ionized (doubly-ionized or less), this approximation breaks down. If we wait for the C plasma to expand and cool even more and observe the plasma 15 ns after the time of plasma creation we observed most of the fringes moving to the left. The interferometer and experimental configuration are described in more detail in Refs. 14 and 15. In the next two sections we will describe the methods used to calculate the index of refraction for the C plasmas and the results from those calculations.

3. Calculational methods

In this paper we compare three different methods to calculate the index of refraction for carbon plasmas near C^{2+}. The first method, called AVATOMKG for average-atom Kubo-Greenwood, is very general and enables one to calculate the index of refraction for any plasma at any wavelength by using a modified version of the INFERNO average atom code. The INFERNO code [21] has been used for many years to calculate the ionization conditions and absorption spectrum of plasmas under a wide variety of conditions. For given temperatures and densities, the INFERNO code calculates a statistical population for occupation of one-electron Dirac orbitals in the plasma. In this work, the AVATOMKG method uses a non-relativistic version of INFERNO to calculate bound and continuum orbitals and the corresponding self-consistent potential. By applying linear response theory we obtain an average-atom version of the Kubo-Greenwood equation [25,26] for the frequency-dependent conductivity of the plasma. The imaginary part of the complex dielectric function is proportional to the conductivity. The real part of the dielectric function can be found from its imaginary part using a Kramers-Kronig [24] dispersion relation. The details of the Kubo-Greenwood formula applied to the average-atom model are described in Ref . 20.

The average atom version of the Kubo-Greenwood formula described in Ref. 20 diverges at low frequencies, where the single-atom approximation, which presumes that scattering of a conducting electron on each atom takes place independently of all other atoms, fails. The relaxation time τ distinguishes a relatively high-frequency region $\omega\tau > 1$, where the one-atom approximation is applicable explicitly, from extreme low frequencies $\omega\tau < 1$, where the one-atom approximation breaks down. In this work, we use a modified version of the formalism, which takes into account the many-atomic collisions and is found to be accurate in all frequency regions, from $\omega=0$ to $\omega\tau >>1$. The present version of the AVATOMKG code reproduces the Ziman formula in the static limit, reproduces the results based on the previous version of the Kubo-Greenwood formula for high frequencies, and satisfies the conductivity sum-rule.

When we originally developed the AVATOMKG code we validated the results for partially ionized Al plasmas against calculations done with the OPAL code [27-29], which is the second method used in this paper. The OPAL code was developed at the Lawrence Livermore National Laboratory to compute opacities of low- to mid-Z elements. The calculations are based on a physical picture approach that carries out a many-body expansion of the grand canonical partition function. The method includes electron degeneracy and the leading quantum diffraction term as well as systematic corrections necessary for strongly-coupled plasma regimes. The atomic data are obtained from a parametric potential method that is fast enough for in-line calculations while achieving accuracy comparable to single configuration Hartree-Fock results. The calculations use detailed term accounting; for example, the bound-bound transitions are treated in full intermediate or pure LS coupling depending on the element. Degeneracy and plasma collective effects are included in inverse Bremsstrahlung and Thomson scattering. Most line broadening is treated with a Voigt profile that accounts for Doppler, natural width, and electron impacts. Linear Stark broadening by the ions is included for one-, two-, and three-electron systems. By contrast to the average-atom approach, where ions are assumed to be fractionally occupied, in the OPAL code the plasma is treated as a mixture of atoms in discrete ionization states, thereby giving a more realistic description of individual lines and absorption edges. However the OPAL calculations can only be done for a limited range of ions. The OPAL calculations do include full spin-orbit coupling.

Our third method is an old method first used by Castor, Abbott, and Klein in 1974 to provide C^{2+} data for calculations of solar winds [30]. We refer to this method as CAK after the first letters of the authors' last names. The set of energy level and oscillator strength data used by CAK was calculated using the multi-channel quantum defect theory developed by Seaton and others [31]. The

method used for the C^{2+} data in CAK was to fit the 1-channel or 3-channel scaled R matrices to analytic functions of energy such that the poles of the corresponding S-matrices agreed with the tabulated energy levels published by NIST [32]. This gives results for all the configuration-interaction (CI) mixing coefficients. A Bates-Damgaard-like procedure is used to estimate the radial integrals for all the transitions, which, with the mixing coefficients, give the line strengths S. Most of the transition energies agree with the experimental values, but the unmeasured lines are predicted from the R-matrix fits.

The CAK calculation includes 134 levels with 2snl and 2pnl configurations from n = 2 to 6 for C^{2+}. There is no spin-orbit splitting included. The line strength S is the square of the reduced matrix element summed over all the transitions in a group, such as the ^3P multiplet. The dipole line strength is conventionally quoted in atomic units of $(a_0*e)^2$ where a_0 is the Bohr radius of 5.29×10^{-9} cm. The absorption oscillator strength f_{osc} is related to the absorption opacity in a line or in a blended group of lines. The relation between the electric dipole line strength S and the absorption oscillator strength f_{osc} is given $f_{osc} = \Delta E\ S / [3\ g_{lower}]$ where ΔE is the transition energy in Rydberg (Ry = 13.60583 eV) and g_{lower} is the statistical weight of the lower energy level for the transition. For an LS term, g_{lower} is (2S+1)(2L+1), so if we consider an example such as the $2s2p(^3P) \rightarrow 2s3d(^3D)$ transition in C^{2+} then the lower ^3P level has $g_{lower} = 9$ since L = 1 and S = 1 for a ^3P state. The CAK calculation has dipole line strength S and the transition energy ΔE calculated for each transition. We convert f_{osc} into the absorption coefficient f_2 used in Eq. (3) by $f_2 = (\pi/2)\ \Delta E\ f_{osc}\ g(\varepsilon)$ where $g(\varepsilon)$ is the lineshape such that the integral of $g(\varepsilon)\ d\varepsilon$ is normalized to unity. For a Lorentzian lineshape $g(\varepsilon) = (2\ a / \pi) / [\Delta E^2 + a^2]$ where a is the half-width half-maximum linewidth. In this paper we set a = 0.088 eV based on the OPAL calculations done with a temperature of 6 eV and an ion density of 10^{20} cm^{-3}. We also use a linewidth multiplier of 3.52 in the AVATOMKG calculations to make those calculations have the same linewidth as the OPAL calculations. When one uses f_2 in the Eq. (3) the contribution to f_1 at photon energy E due to a single line with absorption oscillator strength f_{osc} and transition energy ΔE is

$$\Delta f_1(E) = (E - \Delta E)\ \Delta E^2\ f_{osc} / [(E + \Delta E)\ ((E - \Delta E)^2 + a^2)]. \quad (4)$$

This formula insures that the contribution to f_1 at energy E = 0 is $-f_{osc}$ for a single line. In order to get the total contribution for N_{ion} C^{2+} ions to the index of refraction we calculated a Boltzmann distribution for the fractional population in each energy level by first creating a $SUM = \Sigma_i\ g_i \exp(-E_i/\theta)$ for all the energy levels i with statistical weight g_i and energy E_i of C^{2+} where $\theta = kT$ is the

temperature in energy units. For each transition the contribution to f_1 shown above is then modified by the fractional population in the lower energy level, $g_i \exp(-E_i/\theta)$ / SUM, times the relative population in the transition, $1 - \exp(-\Delta E/\theta)$. This last term is a very small effect for the calculations done in this paper. We sum over all the transitions in the CAK calculation. To calculate the final value of f_1 after including all the transitions we add a constant value of 3.04 to f_1 to force $f_1 = 2.0$ at $E = 0$. This added constant represents the bound-free transitions for the K and L shell as well as the higher energy bound transitions associated with the K shell such as 1s – 2p. Since these transitions are all at higher energy their contribution to f_1 at lower energies tend to be a constant value.

4. Modeling of carbon plasmas

Several years ago our calculations showed that the index of refraction of partially ionized C plasma was very complex for photon energies below 40 eV [18]. To understand what C plasmas would display an anomalous index of refraction near 47 nm we first need to look at the absorption characteristics of C. For neutral C the ionization potential is at 11.26 eV. This L shell absorption edge moves to 24.38 eV for singly ionized C, which would be a very opaque plasma for the 26.44 eV X-ray laser, since the laser is just above this absorption edge. However the ionization potential for doubly ionized C moves to 47.89 eV, which makes the plasma quite transparent for this X-ray laser, which is now far below the absorption edge. As we continue to ionize C the ionization potential moves to even higher energy. Since absorption is an issue for neutral and singly ionized C we used the AVATOMKG average atom code to calculate the index of refraction for C^{2+}, C^{3+}, and C^{4+}, by using an ion density of 10^{20} cm^{-3} and plasma temperatures of 6, 10, and 30 eV to achieve $Z^* = 1.97$, 2.92, and 3.95, respectively. Z^* is the average degree of ionization so that $Z^* = 2$ means the plasma is doubly ionized, on average. The optical constants that we calculate are dimensionless and therefore independent of the actual density of the plasmas. Since the main feature in the spectrum are the 2p – 3d lines in each of these ionization stages we shifted the energy scale of the AVATOMKG results to make sure that the photon energy of the main absorption feature agreed with the experimentally observed energies. This required a positive shift of 4.21, 1.95, and 13.3 eV for C^{2+}, C^{3+}, and C^{4+}, respectively. It is typical to have to make shifts in the energy scale to make atomic calculations align with experimental data so it is vital to have at least one experimentally measured line to benchmark the calculations against. Figure 2a shows the optical constant f_1 versus photon energy calculated by the AVATOMKG code for these three ionization stages. One observes

that f_1 is negative (-5.6) at 26.44 eV for the C^{2+} (solid line). As the 2p – 3d line shifts to higher energy for C^{3+}(dashed line), f_1 is 2.2 at 26.44 eV. As one continues to ionize the plasma to C^{4+} (dotted line), f_1 approaches 4 over this entire energy range as the contribution from the bound electrons disappear.

Using the OPAL code we did similar calculations of C plasmas with temperatures of 6, 10, and 30 eV. This gave Z* = 1.93, 2.96, and 3.90, respectively. For the 6 eV temperature case we shifted the energy scale of the OPAL calculations by -0.35 eV to make the dominant 2p-3d line in C^{2+} agree with the measurement. For the 10 and 30 eV plasmas we shifted the energy scale by -0.2 eV to make the dominant 2p-3d line in C^{3+} agree with the measurement. Figure 2b plots the optical constant f_1 versus photon energy calculated by the OPAL code for the C plasmas with these three temperatures that result in the average ionization stages being near C^{2+}, C^{3+}, and C^{4+}, respectively. Comparing Figs. 2a and 2b one can see a lot of similarity in the results. The value of f_1 is negative (-0.8) at 26.44 eV for the C^{2+} (solid line) and becomes positive (2.4) for C^{3+}(dashed line). As one continues to ionize the plasma to C^{4+} (dotted line), f_1 is 3.9 at 26.44 eV and approaches 4 over this entire energy range as the contribution from the bound electrons disappear.

Comparing Figs. 2a and 2b one can see the big difference between the two methods. For the average atom method there is one strong 2p – 3d line that moves to higher energy as the plasma becomes more ionized while in the OPAL calculation one can see the 2p – 3d line near 27 eV in C^{2+} become weaker and the 2p – 3d line near 32 eV in C^{3+} become stronger as the plasma becomes more ionized. For the OPAL calculation both lines are present in both plasmas but the relative strength changes. Figure 3 highlights this difference by plotting the optical constant f_1 versus photon energy for the 10 eV plasma with Z* near 3 for both the AVATOMKG(solid line) and OPAL(dashed line) codes. For the strong 2p – 3d line in C^{3+} at 32.28 eV the two codes agree well. Even for the weaker 2p – 3s line at 29.55 eV the two codes agree except for the AVATOMKG code having the line at 29 eV. However, for the AVATOMKG code the C^{2+} lines near 25 and 27 eV have disappeared while the OPAL calculation still has these lines present but they are much weaker due to the small population of C^{2+} ions at this higher plasma temperature. Clearly C^{2+} is the important ionization stage for looking at the anomalous dispersion in C plasmas for the interferometer experiments done with the X-ray laser at 26.44 eV because of the strong 2p – 3d line near 27 eV, so we focus on C^{2+} in the rest of this paper. It is also clear from the OPAL calculation that even though there is a

distribution of ionization stages, at a temperature of 6 eV, the C^{2+} ionization stage dominates in the calculation.

For C^{2+} we now calculate f_1 using the CAK method described in the previous section and compare with the AVATOMKG and OPAL calculations. For a C plasma with a temperature of 6 eV the AVATOMKG average atom code has Z* = 1.97 and OPAL has 1.93 while the CAK method only includes C^{2+} transitions. Fig. 4 shows f_1 versus photon energy for a 6 eV C plasma using the three different methods. At 26.44 eV f_1 is -5.6 for average atom(solid line), -3.8 for CAK(dashed line), and -0.8 for OPAL(dashed line). In all three cases the calculations have negative f_1 at 26.44 eV which means we would measure an index of refraction larger than one and see the fringe lines bend the opposite direction as would usually be expected. However there are large differences in the absolute value of f_1 so there is still a lot of improvement that can be made.

To understand some of the other detailed spectral differences between the methods Fig. 5 plots the absorption constant f_2 versus photon energy for the C plasma with temperature of 6 eV for the AVATOMKG (solid line) and CAK (dotted line) calculations. For the AVATOMKG calculation one observes two significant lines, the 2p – 3s line at 23.38 eV, and the 2p – 3d line at 26.99 eV. Looking at experimental data the dominant 2p-3s line is measured near 23.04 eV, so the AVATOMKG calculation has the energy about 0.3 eV too high but the CAK result is in excellent agreement. The AVATOMKG 2p-3d line agrees with the measured line at 26.978 eV since we shifted the AVATOMKG spectra 4.21 eV to force agreement for this line.

Now let us look in more detail at the 2p-3d line at 26.98 eV (45.96 nm). In the AVATOMKG calculation this is a single line with $f_{osc} = 0.35$. For the CAK method this single configuration-averaged line is divided into seven configuration-specific lines, as shown in Table 1. Listed in Table 1 is the transition in LS coupling, wavelength, energy, f_{osc}, and fractional population in the lower level of the transition for a plasma with a temperature of 6 eV. All these lines can be seen clearly in Fig. 5 except for the 23.162 eV line which is hidden on the high energy shoulder of the stronger 2p-3s line at 23.036 eV. Even though most of the lines have a large f_{osc} the line at 26.978 eV dominates because it has a much larger fractional population in the lower level of the transition. In the AVATOMKG calculation all the population is in the lower level because there is only one lower level. Therefore the AVATOMKG calculation gives very good agreement with the CAK method when calculating f_1 because the single line in the AVATOMKG calculation dominates the results. To determine the effective oscillator strength in the CAK calculation one takes the product of f_{osc}

and the fractional population in the lower level listed in Table 1. If one was looking at the effect from any of the other six weaker lines the AVATOMKG code would be missing those lines and we would need another general method like OPAL or specific detailed method like CAK.

The OPAL method includes all the lines including the spin-orbit coupling. To highlight this difference lets look at the 2s2p(^{3}P)-2s3d(^{3}D) line at 26.978 eV from the CAK calculation. This single line can be further broken down into five separate lines [32] when the total angular momentum J for the spin-orbit coupling is included, as shown in Table 2. For the CAK calculation the $g_i = 9$ for the lower ^{3}P having L=1 and S=1. This is broken into 3 energy levels with J = 0, 1, and 2 which have a total degeneracy of 9. One notices that these separate lines are not visible in the calculation because they are all within 0.01 eV of each other while our calculations have a full-width half maximum (FWHM) linewidth of 0.176 eV, which is much larger. If one sums the f_{osc} to different upper states and averages over the lower states weighted by their statistical weight one can determine an average $f_{osc} = 0.558$ for these lines which is about 94% of the value calculated by the CAK method. The big difference with the OPAL method is that there is a distribution of ionization stages and therefore we have lines from different ionization stages present.

5. Conclusions

For decades, diagnostics of multiply ionized plasmas such as interferometry and refractometry have relied on the approximation that the index of refraction in plasmas is due solely to the free electrons. This approximation makes the index of refraction less than one and is an essential assumption for using interferometers to directly measure electron densities in plasmas. This assumption is also used in determining the critical density surface for energy deposition in a plasma and for doing photon transport calculations. Recent X-ray laser interferometer measurements of Al, Sn, Ag, and C plasmas observed anomalous results with the index of refraction being greater than one. The analysis of the plasmas showed that the anomalous dispersion from both the resonance lines and absorption edges due to the bound electrons can be the dominant contribution to the index of refraction over the photon range from the optical up to 100 eV (12 nm) soft X-rays.

In this paper we have used three different methods to calculate the index of refraction for doubly ionized C plasmas and have discussed the approximations used and the importance of

experimental atomic data to benchmark the codes against. We show that the average atom (AVATOMKG) approach works well when the effects of the strongest lines dominate the dispersion but that the more detailed calculations such as OPAL and CAK are essential to evaluate the effect of weaker lines in the plasma. We also present experimental data that observes the index of refraction greater than one in a carbon plasma at the 46.9 nm (26.44 eV) wavelength of the Ne-like Ar X-ray laser.

X-ray laser interferometers are a valuable tool to measure the index of refraction and electron density of plasmas. During the next decade X-ray free electron lasers and other sources will be available to probe a wider variety of plasmas at higher densities and shorter wavelengths so it will be even more essential to understand the index of refraction in plasmas. With the advent of tunable X-ray lasers, the frequency dependent interferometry measurements of the index of refraction may enable us to determine the absorption coefficients and lineshapes and make detailed comparisons against our atomic physics codes.

Acknowledgements

This work performed under the auspices of the U.S. Department of Energy by Lawrence Livermore National Laboratory under Contract DE-AC52-07NA27344. This research was also sponsored by the National Nuclear Security Administration under the Stewardship Science Academic Alliances program through U. S. Department of Energy Research Grant # DE-FG52-06NA26152, using the facilities from the NSF ERC for Extreme Ultraviolet Science and Technology, Grant No. EEC-0310717. The work of one author (WRJ) was supported in part by NSF Grant No. PHY-0456828.

REFERENCES

[1] G. J. Tallents, J. Phys. D. **17**, 721 (1984).

[2] H. R. Griem, *Principles of Plasma Spectroscopy*, (Cambridge University Press, Cambridge, 1997) p. 9

[3] L. B. Da Silva, T. W. Barbee, Jr., R. Cauble, P. Celliers, D. Ciarlo, S. Libby, R. A. London, D. Matthews, S. Mrowka, J. C. Moreno, D. Ress, J. E. Trebes, A. S. Wan, and F. Weber, Phys. Rev. Lett. **74**, 3991 (1995).

[4] F. Albert, D. Joyeux, P. Jaegle, A. Carillon, J. P. Chauvineau, G. Jamelot, A. Klisnick, J. C. Lagron, D. Phalippou, D. Ros, S. Sebban and P. Zeitoun, Opt. Comm. **142**, 184 (1997).

[5] J.J Rocca, C.H. Moreno, M.C Marconi, and K. Kanizay, Opt. Lett. **24**, 420 (1999).

[6] J. Filevich, K. Kanizay, M. C. Marconi, J. L. A. Chilla, and J. J. Rocca, Opt. Lett **25**, 356 (2000).

[7] D. Descamps, C. Lyngå, J. Norin, A. L'Hullier, C.-G. Wahlström, J.-F. Hergott, H. Merdji, P. Salières, M. Bellini, and T. W. Hänsch, Opt. Lett. **25**, 135 (2000).

[8] J. Filevich, J. Rocca, M. Marconi, R. Smith, J. Dunn, R. Keenan, J. Hunter, S. Moon, J. Nilsen, A. Ng, and V. Shlyaptsev, Appl. Opt. **43**, 3938 (2004).

[9] A. Meseck, M. Abo-Bakr, D. Krämer, B. Kuske, and S. Reiche, Nucl. Inst. and Meth. A **528**, 577 (2004).

[10] H. Tang, O. Guilbaud, G. Jamelot, D. Ros, A. Klisnick, D. Joyeux, D. Phalippou, M. Kado, M. Nishikino, M. Kishimoto, K. Sukegawa, M. Ishino, K. Nagashima, and H. Daido, Appl. Phys. B **78**, 975 (2004).

[11] J. Filevich, J. J. Rocca, M. C. Marconi, S. Moon, J. Nilsen, J. H. Scofield, J. Dunn, R. F. Smith, R. Keenan, J. R. Hunter, and V. N. Shlyaptsev, Phys. Rev. Lett. **94**, 035005 (2005).

[12] J. Filevich, J. J. Rocca, M. C. Marconi, S. Moon, J. Nilsen, J. H. Scofield, J. Dunn, R. F. Smith, R. Keenan, J. R. Hunter, and V. N. Shlyaptsev, J. Quant. Spectrosc. Radiat. Transfer **99**, 165 (2006).

[13] J. Filevich, J. Grava, M. Purvis, M. C. Marconi, J. J. Rocca, J. Nilsen, J. Dunn, W. R. Johnson, Phys. Rev. E **74**, 016404 (2006).

[14] J. Filevich, J. Grava, M. Purvis, M. C. Marconi, J. J. Rocca, J. Nilsen, J. Dunn, W. R. Johnson, Laser and Particle Beams **25**, 47 (2007).

[15] M. Purvis, J. Grava, J. Filevich, M. C. Marconi, J. Dunn, S. J. Moon, V. N. Shlyaptsev, E. Jankowska, and J. J. Rocca, Phys. Rev. E **76**, 046402 (2007).

[16] J. Nilsen and J. H. Scofield, Opt. Lett. **29**, 2677 (2004).

[17] J. Nilsen and W. R. Johnson, Appl. Opt. **44**, 7295 (2005).

[18] J. Nilsen, W. R. Johnson, C. A. Iglesias, and J. H. Scofield, J. Quant. Spectrosc. Radiat. Transfer **99**, 425 (2006).

[19] M. Born and E. Wolf, *Principles of Optics*, (Pergamon Press, New York, 1984) pp. 90 - 98

[20] W. R. Johnson, C. Guet, and G. F. Bertsch, J. Quant. Spectrosc. Radiat. Transfer **99**, 327 (2006).

[21] D. A. Liberman, JQSRT **27**, 335 (1982).

[22] J. J. Rocca, V. Shlyaptsev, F. G. Tomasel, O. D. Cortázar, D. Hartshorn, and J. L. A. Chilla, Phys. Rev. Lett. **73**, 2192 (1994).

[23] B. L. Henke, E. M. Gullikson, and J. C. Davis, ADNDT **54**, 181 (1993).

[24] L. D. Landau and E. M. Lifshitz, *Electrodynamics of Continuous Media*, (Pergamon, New York, 1984) pp. 280 - 283

[25] D. A. Greenwood, Proc. Phys. Soc. London **715**, 585 (1958).

[26] R. Kubo, J. Phys. Soc. Jpn. **12**, 570 (1957).

[27] C. A. Iglesias, F. J. Rogers, and B. G. Wilson, Astrophys. J. Lett. **322**, L45 (1987).

[28] F. J. Rogers, B. G. Wilson, and C. A. Iglesias, Phys. Rev. A **38**, 5007 (1988).

[29] C. A. Iglesias and F. J. Rogers Astrophys. J. **464**, 943 (1996).

[30] J. I. Castor, D. C. Abbott, R. I. Klein, Astrophys. J., **195**, 157 (1975).

[31] M. J. Seaton, Rep. Prog. Phys. **46**, 167 (1983).

[32] NIST web site at http://physics.nist.gov/PhysRefData/ASD/index.html

Figure and table captions:

Fig. 1. (a) (top) Interferogram of carbon plasma generated by irradiating a semi-cylindrical cavity and taken at 3 nsec after laser irradiation. Fringes in the middle of the plasma are bending to the right however fringes near the target surface are bending to the left of the reference fringes (solid lines) indicating an index of refraction larger than one even at this early time. The target surface is shown by the white line on the left side of the figure. (b) (bottom) Fringe shift map corresponding to the interferogram of (a).

Fig. 2. (a) Optical constant f_1 versus photon energy calculated with the average atom code (AVATOMKG) for three different ionization stages of carbon plasmas. (b) Optical constant f_1 versus photon energy calculated with the OPAL code for three different ionization stages of carbon plasmas.

Fig. 3. Optical constant f_1 versus photon energy calculated with the average atom (AVATOMKG) and OPAL codes for carbon plasmas at a temperature of 10 eV, whose degree of ionization is near C^{3+}.

Fig. 4. Optical constant f_1 versus photon energy calculated with the AVATOMKG, OPAL, and CAK codes for carbon plasmas at a temperature of 6 eV, whose degree of ionization is near C^{2+}.

Fig. 5. Absorption constant f_2 versus photon energy calculated with the AVATOMKG and CAK codes for carbon plasmas at a temperature of 6 eV, whose degree of ionization is near C^{2+}.

Table 1. The seven 2p-3d lines in the CAK calculation showing wavelength, photon energy, f_{osc}, and the fractional population in the lower state of the transition at a plasma temperature of 6 eV.

Table 2. The five fine structure lines from the single $2s2p(^3P)$-$2s3d(^3D)$ transition.

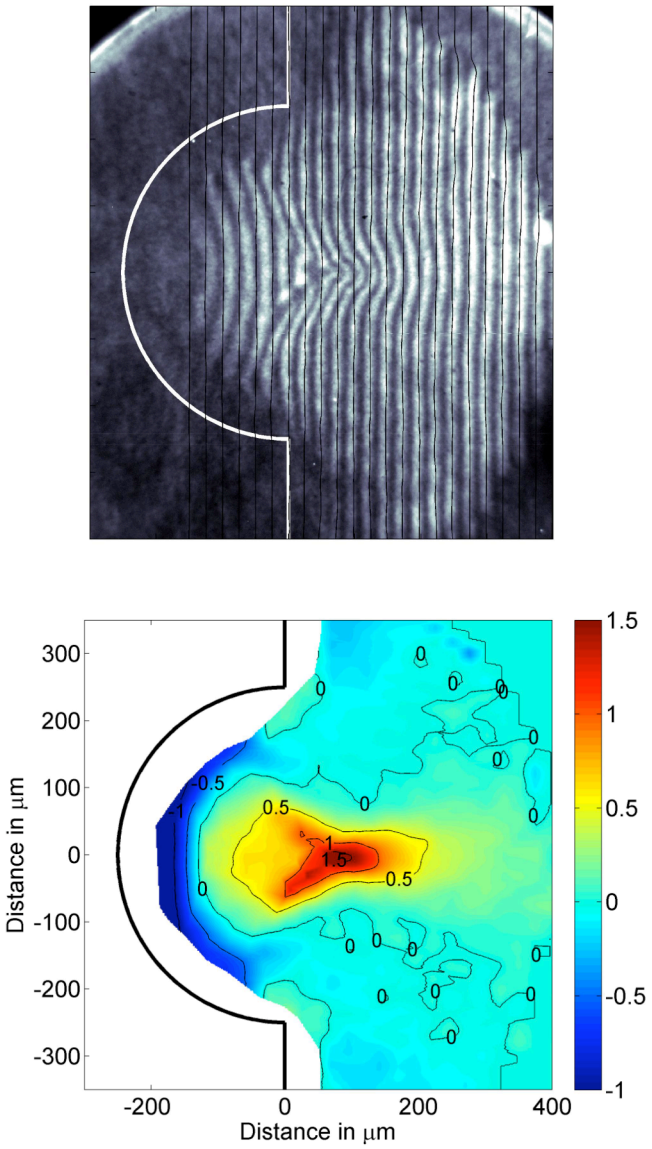

Fig. 1. (a) (top) Interferogram of carbon plasma generated by irradiating a semi-cylindrical cavity and taken at 3 nsec after laser irradiation. Fringes in the middle of the plasma are bending to the right however fringes near the target surface are bending to the left of the reference fringes (solid lines) indicating an index of refraction larger than one even at this early time. The target surface is shown by the white line on the left side of the figure. (b) (bottom) Fringe shift map corresponding to the interferogram of (a).

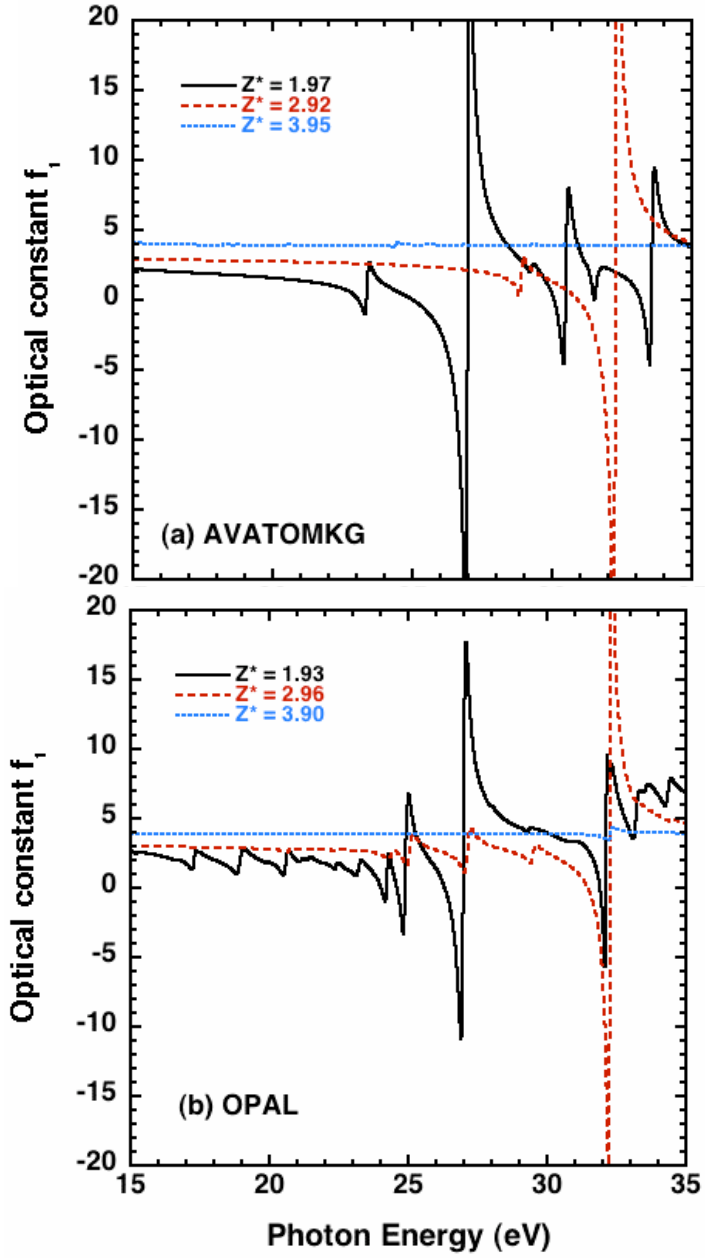

Fig. 2. (a) Optical constant f_1 versus photon energy calculated with the average atom code (AVATOMKG) for three different ionization stages of carbon plasmas. (b) Optical constant f_1 versus photon energy calculated with the OPAL code for three different ionization stages of carbon plasmas.

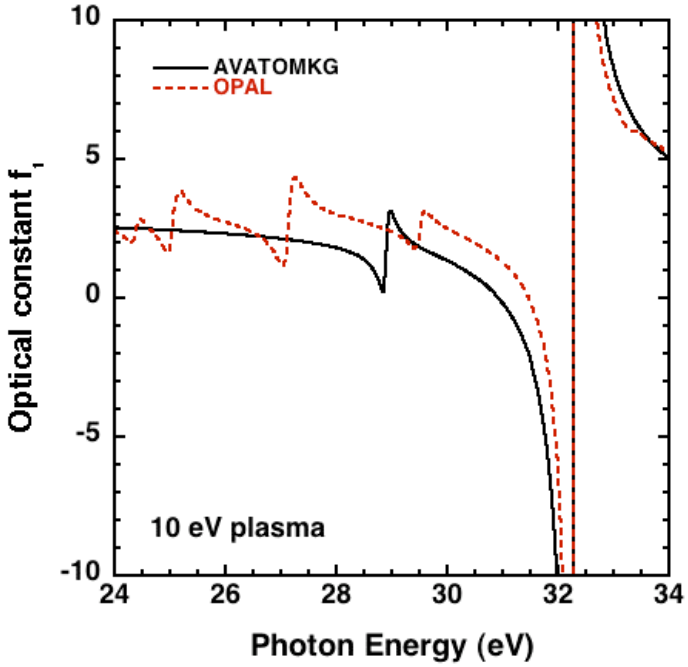

Fig. 3. Optical constant f_1 versus photon energy calculated with the average atom (AVATOMKG) and OPAL codes for carbon plasmas at a temperature of 10 eV, whose degree of ionization is near C^{3+}.

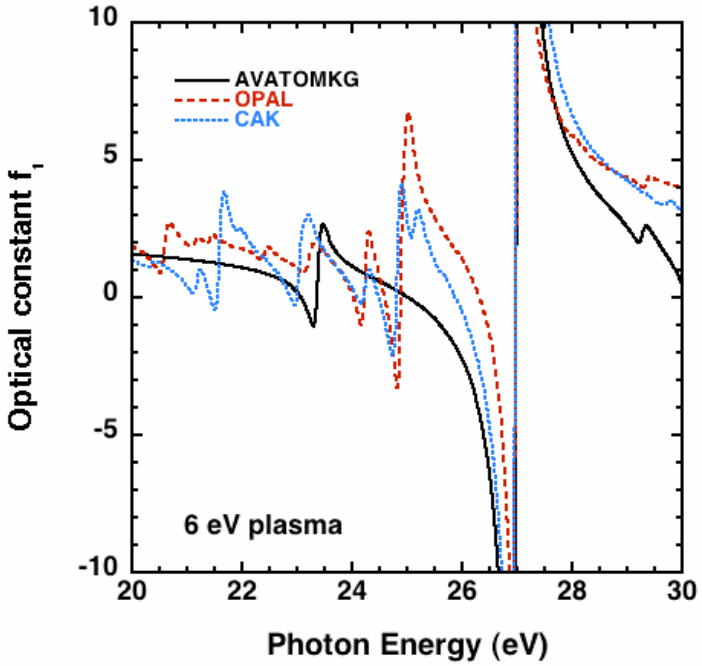

Fig. 4. Optical constant f_1 versus photon energy calculated with the AVATOMKG, OPAL, and CAK codes for carbon plasmas at a temperature of 6 eV, whose degree of ionization is near C^{2+}.

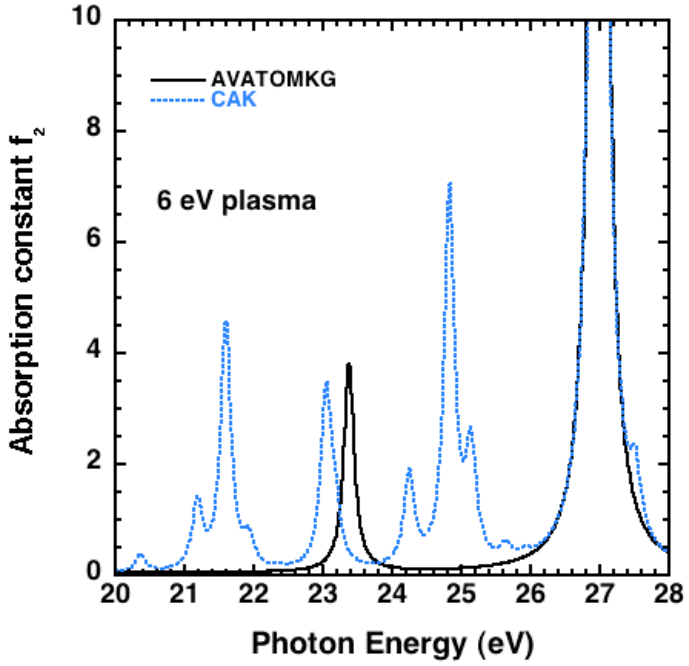

Fig. 5. Absorption constant f_2 versus photon energy calculated with the AVATOMKG and CAK codes for carbon plasmas at a temperature of 6 eV, whose degree of ionization is near C^{2+}.

Table 1. The seven 2p-3d lines in the CAK calculation showing wavelength, photon energy, f_{osc}, and the fractional population in the lower state of the transition at a plasma temperature of 6 eV.				
Transition	Wavelength(nm)	Energy(eV)	f_{osc}	Fraction
2p2p(^{1}S)-2p3d(^{1}P)	60.904	20.358	0.489	0.0038
2s2p(^{1}P)-2s3d(^{1}D)	57.428	21.590	0.633	0.0593
2p2p(^{1}D)-2p3d(^{1}D)	53.529	23.162	0.183	0.0402
2p2p(^{1}D)-2p3d(^{1}F)	51.152	24.239	0.304	0.0402
2p2p(^{3}P)-2p3d(^{3}D)	49.951	24.822	0.566	0.0861
2p2p(^{3}P)-2p3d(^{3}P)	49.349	25.124	0.139	0.0861
2s2p(^{3}P)-2s3d(^{3}D)	45.957	26.978	0.591	0.4992

Table 2. The five fine structure lines from the single $2s2p(^3P)$-$2s3d(^3D)$ transition.			
Transition	Wavelength(nm)	Energy(eV)	f_{osc}
$2s2p(^3P_0)$-$2s3d(^3D_1)$	45.9466	26.9847	0.564
$2s2p(^3P_1)$-$2s3d(^3D_2)$	45.9514	26.9819	0.422
$2s2p(^3P_1)$-$2s3d(^3D_1)$	45.9516	26.9817	0.141
$2s2p(^3P_2)$-$2s3d(^3D_3)$	45.9627	26.9752	0.470
$2s2p(^3P_2)$-$2s3d(^3D_2)$	45.9633	26.9749	0.084